Computational Comparison of Acetate and Nitrate Chemical Ionization of Highly Oxidized Cyclohexene Ozonolysis Intermediates and Products

Hyttinen, Noora

2017-03-16

Hyttinen , N , Rissanen , M P & Kurten , T 2017 , ' Computational Comparison of Acetate and Nitrate Chemical Ionization of Highly Oxidized Cyclohexene Ozonolysis Intermediates and Products ' , Journal of Physical Chemistry A , vol. 121 , no. 10 , pp. 2172-2179 . https://doi.org/10.1021/acs.jpca.

http://hdl.handle.net/10138/307393
https://doi.org/10.1021/acs.jpca.6b12654

acceptedVersion

Computational Comparison of Acetate and Nitrate Chemical Ionization of Highly Oxidized Cyclohexene Ozonolysis Intermediates and Products

Journal:	*The Journal of Physical Chemistry*
Manuscript ID	jp-2016-12654k.R1
Manuscript Type:	Article
Date Submitted by the Author:	n/a
Complete List of Authors:	Hyttinen, Noora; University of Helsinki, Chemistry Rissanen, Matti; University of Helsinki, Physics Kurtén, Theo; University of Helsinki, Department of Chemistry

Computational Comparison of Acetate and Nitrate Chemical Ionization of Highly Oxidized Cyclohexene Ozonolysis Intermediates and Products

Noora Hyttinen,[a] Matti P. Rissanen,[b] Theo Kurtén[a]*

[a] Department of Chemistry, University of Helsinki, P.O. BOX 55, FI-00014, Helsinki, Finland

[b] Department of Physics, University of Helsinki, P.O. BOX 64, FI-00014, Helsinki, Finland

ABSTRACT During the past few years nitrate chemical ionization has been used to detect highly oxidized products from OH- and O_3-initiated alkene autoxidation. These have been speculated to play a significant role in atmospheric aerosol formation. As less oxidized autoxidation products have not been detected using nitrate chemical ionization, and the absolute concentrations of the highly oxidized species are as yet unknown, other reagent ions, such as acetate, are needed to both verify the detection efficiency of nitrate chemical ionization, and to measure the less oxidized compounds. Here we compare the formation free energies of the acetate and nitrate clusters of several atmospherically relevant RO_2 intermediates and products derived from cyclohexene ozonolysis, calculated at the ωB97xD/aug-cc-pVTZ level of theory.

We found that for the molecules with one hydrogen bonding peroxy acid group, the binding with nitrate is on average 7.5 kcal/mol weaker than with acetate, and the binding is on average 10.5 kcal/mol weaker for molecules with two hydrogen bonding peroxy acid groups. We also calculated the deprotonation energies of the RO_2 intermediates and the closed-shell products, and found that acetate is able to deprotonate almost all of these molecules, while deprotonation with nitrate is (as expected for the conjugate base of a strong acid) not favorable.

INTRODUCTION

According to the latest IPCC report,[1] the largest uncertainty in the radiative forcing of the atmosphere comes from aerosols. A large part of the atmospheric aerosols are secondary organic aerosols (SOA).[2,3] However, there has been a discrepancy between measured and modelled formation and growth rates of SOA, and often the models have underestimated the growth rates compared to the measured ones.[4,5] Recently detected highly oxidized multifunctional compounds, also known as HOMs, derived from the autoxidation of biogenic volatile organic compounds (BVOCs), have been suggested to contribute significantly to both the formation and growth of the SOA.[6,7] Even though the highly oxidized molecules have been included in the modelling of particle growth rates, there is still a discrepancy between measured and modelled rates indicating that current gas-phase measurements likely underestimate the concentrations or formation rates of low-volatility organic compounds in the gas-phase.[8] There are likely many compounds in the ambient air that have yet not been detected with the current gas-phase measurement techniques.[8,9] The under-estimation of SOA concentrations in the large-scale modelling can lead to significant errors in the predictions of radiative forcing.

Recently many different types of neutral molecules, among others HOMs, have been detected in the gas-phase using Chemical Ionization Atmospheric Pressure interface Time-Of-Flight mass spectrometers[10] (CI-APi-TOF). In this instrument, neutral gas-phase sample molecules (RH) are chemically ionized with a reagent ion under atmospheric pressure and temperature. The reagent ion can be either an anion (Q^-) or a cation (QH^+) depending on the compounds that are being measured. In the measurements of oxidized and acidic compounds, a negative ion is most often used:

$$RH + Q^- \underset{R4}{\overset{R1}{\rightleftarrows}} RH(Q^-) \overset{R2}{\rightarrow} QH(R^-) \overset{R3}{\rightarrow} QH + R^-,$$

where R1 is an adduct formation/clustering reaction, R2 is a proton exchange reaction, and the fragmentation reactions, R3 and R4, are deprotonation and declustering, respectively. For smaller molecules, such as H_2SO_4, it is possible that the deprotonation happens before the cluster is stabilized (thermalized) by collisions with gas molecules. In addition to the number and energies of the accessible vibrational modes, and the total pressure, the probability that a cluster is collisionally stabilized also depends on the relative energies of R1 and R3. If the collisional stabilization of the cluster is incomplete, more exothermic clustering reactions (R1) and less endothermic deprotonation reactions (R3) will both lead to higher fractions of deprotonated sample molecules. The ion-molecule clusters studied here all have binding energies of tens of kcal/mol. For the larger molecules that possess many tens of vibrational degrees of freedom, the nascent collision products (i.e. the clusters formed immediately from the ion-molecule collision reaction R1, which still contain all the excess energy of the formation reaction) therefore generally live long enough to be collisionally stabilized. Both deprotonation and declustering will thus occur at their thermal reaction rates (typically on a timescale of at least micro- or milliseconds) rather than on the sub-nanosecond timescale of molecular collisions. The mass

spectrometer is able to detect the neutral sample molecule as either of the clusters, or the deprotonated R^-.

In a system where the reagent ion can form dimers ($QH(Q^-)$), the $RH(Q^-)$ clusters can also be formed by a ligand exchange reaction (R5):

$$QH(Q^-) + RH \overset{R5}{\rightarrow} RH(Q^-) + QH,$$

if the binding of $QH(Q^-)$ is weaker than (or at least not much stronger than) the binding of $RH(Q^-)$. Ligand exchange reactions may also involve other types of reagent ion complexes, such as hydrates: $(H_2O)Q^-$, $(H_2O)_2Q^-$, etc. In systems where the concentration of QH is high and $QH(Q^-)$ strongly bound, the dominant reagent ion is the dimer $QH(Q^-)$, and the difference in the binding energies of $QH(Q^-)$ and $RH(Q^-)$ will determine the sensitivity towards the sample molecule RH.

Nitrate (NO_3^-) was originally used to detect sulfuric acid (H_2SO_4) as a deprotonation product (HSO_4^-), and it was recently noticed to be an especially selective reagent ion also towards highly oxidized organic molecules.[11] It has since been used to detect highly oxidized compounds in both field,[12,13,14,15] and laboratory measurements.[16,17,18] The main detection mechanism with nitrate is cluster formation. Only strong acids, such as H_2SO_4, can also be detected as deprotonated ions.[11]

Acetate ($CH_3C(O)O^-$) chemical ionization has been used in combination with various instruments to measure less oxidized ozonolysis products of for instance α-pinene,[19,20] and other smaller organic acids from the ambient air.[21,22] With acetate ionization, the neutral sample molecules are detected as both clusters and deprotonation products. The method was especially developed to detect atmospherically relevant acids in the gas-phase by proton exchange.[21] Acetate is able to deprotonate acids that have a higher gas-phase acidity than acetic acid, i.e. for which R^- + QH is energetically more favorable than RH + Q^-. If the cluster is very stable, a fraction of the neutral molecules are also detected as clusters. In addition, the deprotonated

sample molecules are able to cluster with other neutral sample molecules.[23] This makes the quantification of the sample molecules more difficult, as one has to account for signals of both the clusters and the deprotonation products.

A combination of laboratory experiments using nitrate chemical ionization and quantum chemical calculations demonstrated the formation of highly oxidized organic compounds from ozone-initiated autoxidation of cyclohexene. [18] A formation mechanism and associated molecular structures were calculated for four closed-shell (a molecule with no unpaired electrons) products, $C_6H_8O_5$, $C_6H_8O_7$, $C_6H_8O_8$ and $C_6H_8O_9$, but only the three latter elemental compositions were actually detected using nitrate chemical ionization. Quantum chemical calculations on the formation free energies of the nitrate clusters of these molecules showed that the binding between the less oxidized closed-shell products and nitrate is weaker than the binding in the reagent ion dimer, $HNO_3(NO_3^-)$.[24] In another laboratory study by Berndt et al,[25] cyclohexene ozonolysis products were measured using both acetate and nitrate ionization. In that study also several open-shell (a molecule with at least one unpaired electron) peroxy radical(RO_2) intermediates, $C_6H_9O_6$ $C_6H_9O_8$ and $C_6H_9O_{10}$, were detected. The detection sensitivity with the two reagent ions was found to be similar, especially towards the highly oxidized RO_2 radicals. They were also not able to detect the closed-shell product with only one hydroperoxy group, $C_6H_8O_5$, using nitrate ionization, but with acetate, this product was detected.

Laboratory experiments comparing acetate and nitrate as reagent ions measuring monoterpene[26] and sesquiterpene[27,28] ozonolysis intermediates have shown that the RO_2 radicals with lower oxygen content have a lower sensitivity using nitrate chemical ionization.[25,28] However, because of the higher background noise, the highly oxidized compounds with low

concentrations are more difficult to detect using acetate.[28] Also, certain closed-shell ozonolysis products have been reported to have a lower sensitivity using acetate than using nitrate.[25,28]

The chemical ionization process has previously been modelled by calculating the binding energies between nitrate and the closed-shell products of cyclohexene ozonolysis.[24] Based on the quantum chemical calculations and measurements[18] with nitrate CI-APi-TOF, it was concluded that at least two hydroperoxy groups are needed for the closed-shell ozonolysis products of cyclohexene to be detected with this instrument.[24] Calculations on smaller RO_2 radicals with varying functional groups show that acetate has a stronger binding (by around 4-11 kcal/mol depending on the radical) than nitrate.[26] The calculations also showed that the binding to reagent ions for species containing a hydroperoxy group is stronger than for those containing a hydroxy group, but carboxylic acids bind even stronger than hydroperoxides. Quantum chemical calculations have also been used to model sensitivities in an iodide based chemical ionization mass spectrometer (CIMS), comparing the binding enthalpies with measured sensitivities. A chemical ionization mass spectrometer with an iodide reagent ion was found to have a maximum sensitivity for molecules that have higher than 26 kcal/mol binding enthalpy with the iodide ion, calculated at the DLPNO-CCSD(T)/def2-QZVPP//PBE/aug-cc-pVTZ-PP level of theory.[29] For the weakest binding closed-shell cyclohexene ozonolysis derived autoxidation product, $C_6H_8O_5$, the formation free energy of the cluster with nitrate is -15.3 kcal/mol (corresponding to a 28.5 kcal/mol binding enthalpy), calculated at the DLPNO-CCSD(T)/def2-QZVPP//ωB97xD/aug-cc-pVTZ level – which should presumably yield similar results.[24] Using nitrate, where the main reagent ion is often the dimer ($QH(Q^-)$), the chemical ionization through ligand exchange (reaction R5) depends on the relative binding energy between the sample molecule and the reagent ion dimer. In contrast, the main reagent ion in an iodide CIMS is likely the monomer (Q^-

), or a weakly bound iodide-water cluster, and thus the sensitivity depends mainly on the absolute binding energy.

Intramolecular H-shifts have been computationally found to be fast between peroxy radical and hydroperoxy groups.[30] As there is a peroxy radical group and one or several hydroperoxy groups in the highly oxidized RO_2 radicals formed in autoxidation, this rapid H-shift scrambling should be taken into account in determining the reaction mechanism of the autoxidation processes. Figure 1 shows the proposed highly oxidized RO_2 radicals derived from cyclohexene ozonolysis[18,25] (left column) and the possible isomers after H-shifts between the peroxy radical group and hydroperoxy groups (on the right).

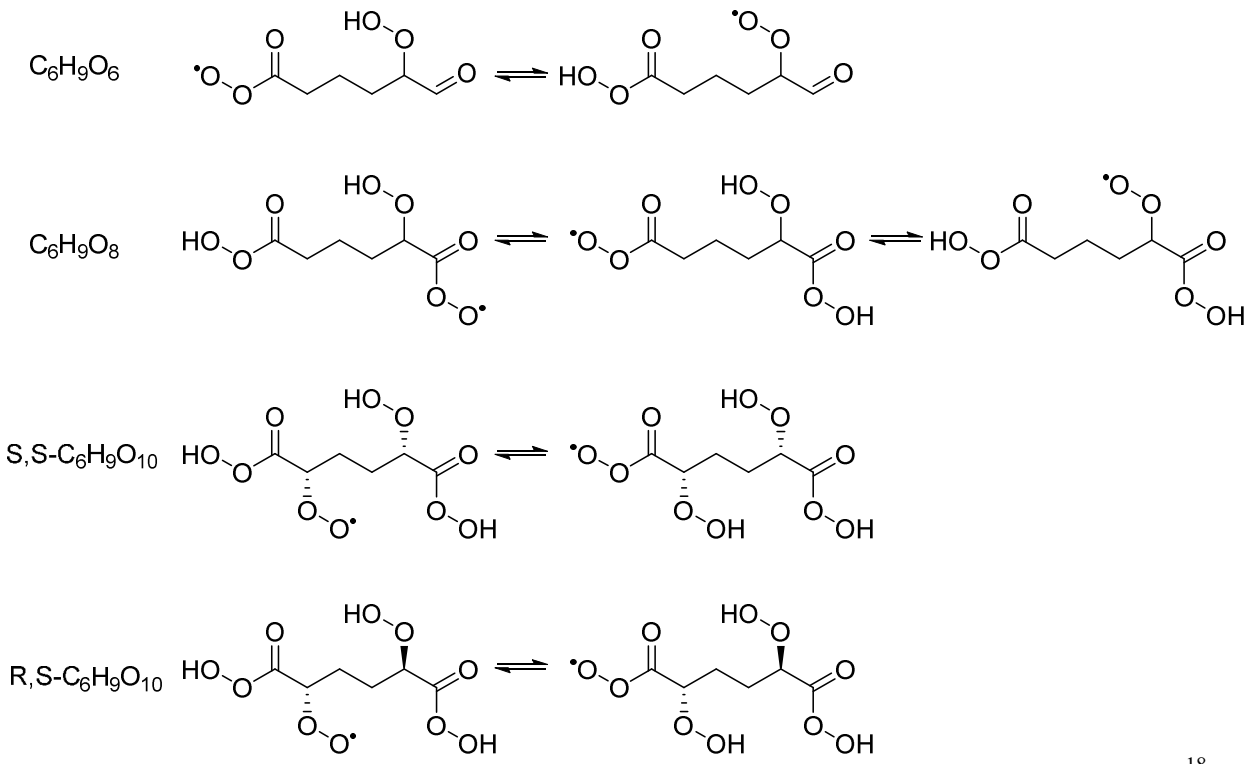

Figure 1 Cyclohexene ozonolysis derived highly oxidized RO_2 radicals by Rissanen et al.[18] on the left column ($C_6H_9O_6$, $C_6H_9O_8$, S,S-$C_6H_9O_{10}$, and R,S-$C_6H_9O_{10}$). On the right are the possible products of rapid H-shift scrambling reactions.

The peroxy radical $C_6H_9O_{10}$ also has two possible diastereomers. Depending on the formation pathway, the ratio of the different diastereomers might vary. Here we first calculate the energies of all of the isomers and diastereomers. We subsequently assume for simplicity that most of this radical is in the lowest-energy isomeric form, and calculate the binding energies to the reagent ions only for that structure. (Binding energy differences between diastereomers are likely to be small as the hydrogen bonding functional groups are identical.) For the smallest RO_2 radical in the study, $C_6H_9O_6$, we also calculate the binding energy of the other isomer in Figure 1 to check how much the change in the functional group positions of the radical affects the binding.

In this study, we compute the lowest-energy conformers of i) all the RO_2 radical isomers described above, ii) acetate and nitrate clusters of the lowest-energy RO_2 radical isomers, iii) acetate clusters of the previously calculated closed-shell species,[24] iv) deprotonation products of the lowest-energy isomers of the two smallest RO_2 radicals and all of the closed-shell molecules v) H_2SO_4 clusters with both acetate and nitrate. With these calculations, we aim to explain the differences in the detection efficiencies of some of the highly oxidized ozonolysis intermediates and products of cyclohexene using acetate and nitrate reagent ions by comparing the computational results with available experimental results.[25]

METHODS

Energy calculations were done similar to a previous study on the binding energies of the closed-shell species with the nitrate reagent ion,[24] allowing us to compare the energies directly. The conformational search was done using MMFF molecular mechanics on Spartan '14.[31] The keyword FFHINT=Ox~~6 (x is the atom number of the radical oxygen) was used for the RO_2 radicals to change the type of the radical oxygen to prevent the MMFF force field from treating it

as an anion.[32] The initial B3LYP/6-31+G* level single-point energies of all of the found conformers were calculated using Spartan‘14. Initial geometry optimizations of all conformers within 5 kcal/mol from the lowest-energy conformer, based on the single-point electronic energies, were calculated with either Spartan ‘14 or Gaussian 09.[33] Using Spartan, duplicates were removed after 10 optimization cycles. For the clusters with less than about 100 conformers, the initial B3LYP optimizations were calculated using Gaussian 09. The final ωB97xD/aug-cc-pVTZ level (aug-cc-pV(T+d)Z[34,35,36] basis set for sulfur) geometry optimization and harmonic frequencies were calculated for all conformers within 2 kcal/mol from the lowest-energy conformer using Gaussian 09 with the ultrafine integration grid. For the free radicals with more than 100 conformers within 2 kcal/mol, the frequencies were only calculated for the conformers within 1 kcal/mol from the lowest ωB97xD/aug-cc-pVTZ electronic energy conformer. Opt=Tight was used for the ωB97xD/aug-cc-pVTZ optimization of the acetate clusters that had an imaginary frequency corresponding to the rotation of the methyl group. In the optimization of the lowest free energy $C_6H_8O_9(CH_3(O)O^-)$ cluster, a superfine integration grid was used to converge the maximum and root mean square forces to zero and the frequencies were calculated at that geometry even though the displacements had not converged. This was necessary to remove a spurious low-lying imaginary vibrational frequency that persisted despite the Opt=Tight setting. (The electronic energy was recomputed at the same geometry using the ultrafine integration grid to keep results comparable).

Final single-point energies on the ωB97xD/aug-cc-pVTZ geometries of the lowest free energy closed-shell molecules and clusters were calculated at the DLPNO-CCSD(T)/def2-QZVPP level of theory using ORCA.[37] DLPNO-CCSD(T)/def2-QZVPP calculations could not be done on the radical species and the cost-effective coupled cluster method used in our previous studies of

autoxidation reactions, ROHF-ROCCSD(T)-F12a/VDZ-F12, proved to be too computationally demanding for even the smallest of the RO_2 intermediates when clustered with a reagent ion. Fortunately, the DLPNO-CCSD(T) corrections to the formation energies of the highly oxidized products are small, and always positive for the acetate clusters and negative for the nitrate clusters, on average 0.8 kcal/mol and -0.4 kcal/mol, respectively. Unless otherwise mentioned, all of the energies presented here are the ωB97xD/aug-cc-pVTZ level Gibbs free energies at 298 K.

Our previous values for the energies of the closed-shell species and their nitrate clusters[24] were used as a starting point of the calculations. However, with the new calculations we found new lowest free energy clusters for some of the sample molecules, see Supporting Information for more details. Also, in our previous calculations the symmetry number of nitrate was incorrectly 1, rather than 6. This leads to an error of around 1 kcal/mol in the Gibbs free energies of formation of all the clusters, which does not affect the conclusions of that paper as the energies relative to the $HNO_3(NO_3^-)$ reagent ion dimer stay the same. For this article we used the correct symmetry number 6 for nitrate.

RESULTS

RO_2 RADICALS

Due to the intramolecular hydrogen bonding of the peroxy acid group, the lowest-energy isomers of the RO_2 radicals are the ones with either one ($C_6H_9O_6$) or two ($C_6H_9O_8$ and $C_6H_9O_{10}$) peroxy acid groups, one peroxy radical group, and zero ($C_6H_9O_6$ and $C_6H_9O_8$) or one ($C_6H_9O_{10}$) hydroperoxy groups. The lowest-energy structures of $C_6H_9O_6$ and $C_6H_9O_8$ are shown on the right-hand-side, and of $C_6H_9O_{10}$ on the left-hand-side in Figure 1. For the smallest RO_2 radical,

$C_6H_9O_6$, the energy difference between the two isomers is the largest, around 10 kcal/mol, and for the larger RO_2 radicals the energy difference is slightly smaller, around 8 kcal/mol. The lower-energy isomer of the R,S-$C_6H_9O_{10}$ diastereomer has around 1 kcal/mol lower energy than the S,S-$C_6H_9O_{10}$ diastereomer.

The binding energies to the reagent ions were calculated for both of the isomers of $C_6H_9O_6$. The hydrogen bonding groups in the higher-energy and lower-energy isomer of $C_6H_9O_6$ are a hydroperoxy group and a peroxy acid group, respectively. As the hydrogen bonding group in the lower-energy isomer is able to form a strong intramolecular hydrogen bond within the peroxy acid group, the binding with the reagent ions is weaker (the hydrogen bond has to be broken in order to form the hydrogen bond with the reagent ion) than for the higher-energy isomer which has no strong intramolecular hydrogen bonds. However, the difference in the binding energies to the reagent ions between the two isomers of that radical is small; only 0.6 kcal/mol with acetate and 1.8 kcal/mol with nitrate.

CLUSTERING ENERGETICS

The formation free energies of the acetate and nitrate clusters are presented in Table 1 and Figure 2. In Figure 2, the formation free energies are drawn relative to the reagent ion dimer ($QH(Q^-)$), and the $H_2SO_4(Q^-)$ free energy has been drawn as reference line, as H_2SO_4 is often used for the concentration calibration of CIMS instruments. The detection efficiency of the highly oxidized molecules is often assumed to be the same as the detection efficiency of H_2SO_4, and the calibration factor derived from H_2SO_4 measurements has been used to obtain lower limit concentrations for the highly oxidized molecules.[25] From the energetics in Table 1 and Figure 2 we can see that H_2SO_4 binds strongly with both acetate and nitrate, and that neither of the reagent

ions bind as strongly with any of the studied highly oxidized molecules. This means that the measured concentrations of the highly oxidized organics are at least not over-estimated if the detection efficiency is assumed to be the same as the detection efficiency of H_2SO_4.

Table 1 The formation free energies (ΔG) of the studied clusters in kcal/mol (at 298.15 K and 1 atm reference pressure) at the ωB97xD/aug-cc-pVTZ level of theory. Note that the results are slightly different from those given in Hyttinen et al.[24] due to the use of the correct symmetry number for the nitrate ion.

	$CH_3C(O)O^-$	NO_3^-
$C_6H_8O_5$	-24.18	-17.08
$C_6H_9O_6$	-26.54	-18.60
$C_6H_8O_7$	-33.51	-23.12
$C_6H_9O_8$	-33.91	-23.49
$C_6H_8O_9$	-38.73	-27.47[24]
$C_6H_9O_{10}$	-37.86	-27.10
Reagent dimer	-17.64	-21.33[24]
H_2SO_4	-43.92	-32.65

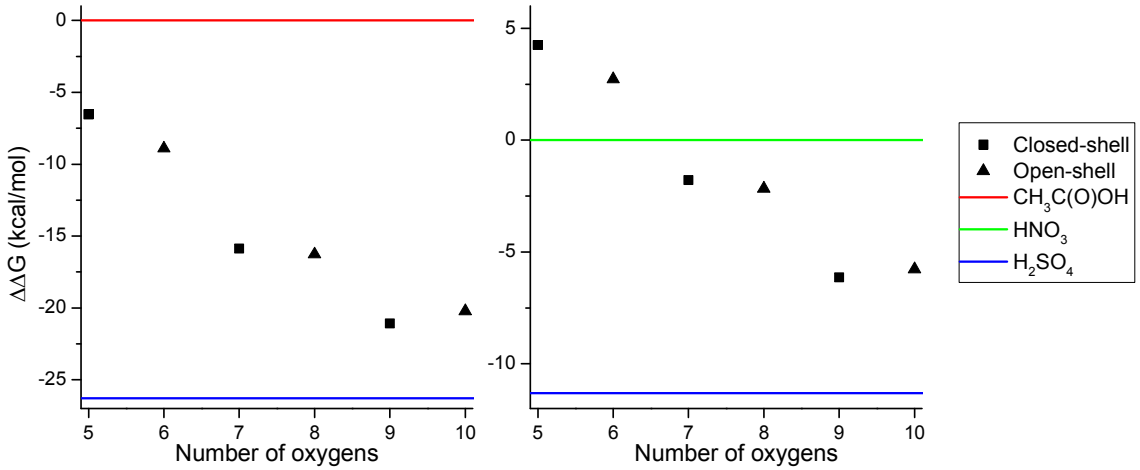

Figure 2 ωB97xD/aug-cc-pVTZ level formation free energies of the acetate (left panel) and nitrate (right panel) clusters, relative to the reagent ion dimer $QH(Q^-)$, in kcal/mol.

The formation free energies follow a similar pattern with both acetate and nitrate, but the binding of the acetate clusters is much stronger than that of the nitrate clusters, around 7.5 and 10.5 kcal/mol for the sample molecules that have one and two peroxy acid groups binding with the reagent ion, respectively. In addition, the binding of the $HNO_3(NO_3)^-$ cluster is much stronger than that of the $CH_3C(O)OH(CH_3C(O)O^-)$ cluster. The ligand exchange reaction (R5) is thus generally less favorable for nitrate than for acetate. Two of the sample molecules are more weakly bound to nitrate than nitric acid is.

The DLPNO-CCSD(T)/def2-QZVPP correction to the ωB97xD/aug-cc-pVTZ electronic energies of the closed-shell products studied here result in on average 0.8 kcal/mol weaker binding for the acetate clusters and 0.4 kcal/mol stronger binding for the nitrate clusters (see Table S1 of Supporting Information), indicating that the ωB97xD/aug-cc-pVTZ level binding energies with acetate are slightly over-estimated and the binding energies with nitrate are slightly under-estimated compared to the coupled cluster energies. The real difference between the two reagent ions is thus likely slightly smaller than indicated by Table 1 and Figure 2.

DEPROTONATION REACTIONS

To investigate the deprotonation process, the energy of the deprotonated lowest-energy isomers of the RO_2 radicals and of all of the closed-shell species, were calculated. Figure 3 shows the lowest-energy conformers of these deprotonation products. In $C_6H_7O_7^-$, $C_6H_8O_8^-$, $C_6H_7O_9^-$, and $C_6H_8O_{10}^-$ the O_2^- group is hydrogen bonded to one or two hydroperoxy groups, making the structure more stable. $C_6H_7O_5^-$ and $C_6H_8O_6^-$ do not have any hydroperoxy groups left after the deprotonation, making the ion relatively less stable. Increasing the number of hydroperoxy groups in the deprotonated sample anion (R^-) from zero to one decreases the free

energy difference between the RH + Q^- and R^- + QH channels by more than 10 kcal/mol due to the formation of a stabilizing intramolecular OO^-…HOO bond in R^-, but the difference between systems with one and two hydroperoxy groups is very small, less than 4 kcal/mol (see Table 2).

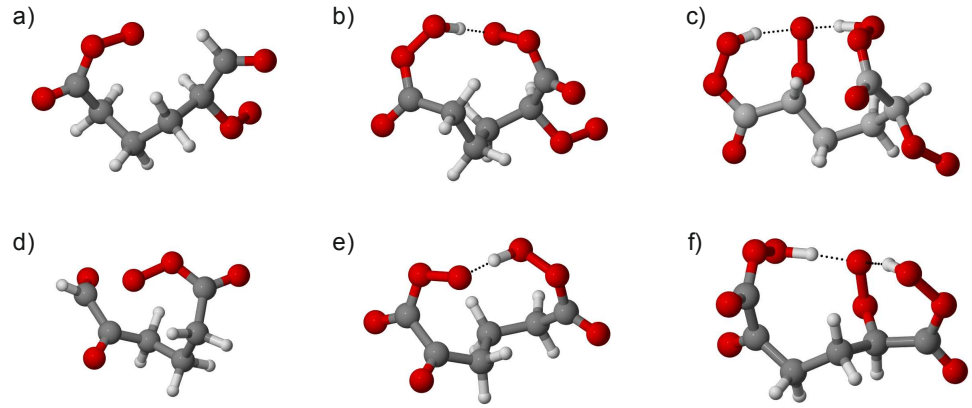

Figure 3 The lowest-energy structures of the deprotonated RO_2 radicals (the peroxy radical groups are on the bottom right corners of the individual structures), a) $C_6H_8O_6^-$, b) $C_6H_8O_8^-$, c) $C_6H_8O_{10}^-$ and closed-shell species, d) $C_6H_7O_5^-$, e) $C_6H_7O_7^-$, f) $C_6H_7O_9^-$. Color coding: grey = carbon, red = oxygen, and white = hydrogen.

Table 2 Free energy and enthalpy differences between the deprotonation products and both the neutral sample molecule and the reagent ion, and the cluster, at the ωB97xD/aug-cc-pVTZ level of theory.

Q	$CH_3C(O)O$				NO_3			
R	RH + Q^- -> R^- + QH		RH(Q^-) -> R^- + QH		RH + Q^- -> R^- + QH		RH(Q^-) -> R^- + QH	
	ΔG	ΔH	ΔG	ΔH	ΔG	ΔH	ΔG	ΔH
$C_6H_7O_5$	-9.07	-13.07	15.11	25.36	13.24	11.23	30.32	40.77
$C_6H_8O_6$	-4.50	-8.18	22.04	32.23	17.81	16.12	36.41	46.85
$C_6H_7O_7$	-20.06	-24.38	13.45	23.76	2.25	-0.09	25.37	34.99
$C_6H_8O_8$	-21.02	-25.85	12.89	22.77	1.30	-1.56	24.79	34.25
$C_6H_7O_9$	-23.68	-27.75	15.04	24.87	-1.37	-3.46	26.09	35.58
$C_6H_8O_{10}$	-24.94	-30.54	12.92	23.27	-2.62	-6.25	24.48	33.58

HSO_4	-34.43	-34.98	9.49	21.62	-12.12	-10.69	20.53	32.20

With acetate, all of the R^- + QH free energies (and enthalpies) are lower than the RH + Q^- energies, making the deprotonation of RH more favorable than the cluster fragmenting into RH + Q^-. However, the free energy needed to fragment the $C_6H_9O_6(CH_3C(O)O^-)$ cluster into $C_6H_8O_6^-$ + $CH_3C(O)OH$ is 22.0 kcal/mol, which is much higher than for the other species. For instance, the free energy difference between the $C_6H_9O_8(CH_3C(O)O^-)$ cluster and the deprotonated radical $C_6H_8O_8^-$ + $CH_3C(O)OH$ is only 12.9 kcal/mol, with the products lying 21.0 kcal/mol below the original reactants $C_6H_9O_8$ + $CH_3C(O)O^-$. If the $C_6H_9O_8(CH_3C(O)O^-)$ cluster fragments, the $C_6H_8O_8^-$ + $CH_3C(O)OH$ channel is thus much more favorable than the $C_6H_9O_8$ + $CH_3C(O)O^-$.

With nitrate, the deprotonation of $C_6H_9O_{10}$ is only 2.6 kcal/mol more favorable than the cluster fragmenting into $C_6H_9O_{10}$ + NO_3^- and the deprotonation of all the other species is even less favorable. Also, all of the energies needed to split the clusters into R^- + QH are much higher with nitrate (QH=HNO_3) than with acetate (QH=$CH_3C(O)OH$).

Figure 4 shows the relative energies between the acetate and nitrate clusters, and the two cluster fragmentation channels. As a reference also data for H_2SO_4 are given, as H_2SO_4 is known to be deprotonated in negative ion mode CI-APi-TOF measurements. The deprotonation of H_2SO_4 with acetate and nitrate is 34.4 kcal/mol and 12.1 kcal/mol more favorable in free energy than the fragmentation of $H_2SO_4(CH_3C(O)O^-)$ and $H_2SO_4(NO_3^-)$ into H_2SO_4 + $CH_3C(O)O^-$ and H_2SO_4 + NO_3^-, respectively.

Reaction dynamic simulations using the MESMER program[38] and similar parameter values that were used in our previous study[39] indicate that under atmospheric conditions the $H_2SO_4(NO_3^-)$ clusters are completely collisionally stabilized, as the yield of products did not change when the total pressure was varied between 1 atm and 10^{-10} atm. The results were not

sensitive to any of the used parameters because of the high energy of the deprotonation reaction. However, a small fraction of the $H_2SO_4(CH_3C(O)O^-)$ clusters may not be collisionally stabilized, because of the large energy difference between $H_2SO_4 + CH_3C(O)O^-$ and $H_2SO_4(CH_3C(O)O^-)$, and the small energy difference between $H_2SO_4(CH_3C(O)O^-)$ and $HSO_4^- + CH_3C(O)OH$. In contrast, our simulations predict full collisional stabilization of the acetate cluster of even the smallest of the organic species studied ($C_6H_7O_5$). The computed energy difference between $RH(Q^-)$ and $R^- + QH$ would need to be wrong by around 10 kcal/mol for this prediction to be wrong. We also note that the rate of collisional stabilization in our simulations is likely to be underpredicted, as the increased collision rate of gas molecules with the clusters due to the presence of charge is not accounted for in the parameter set.

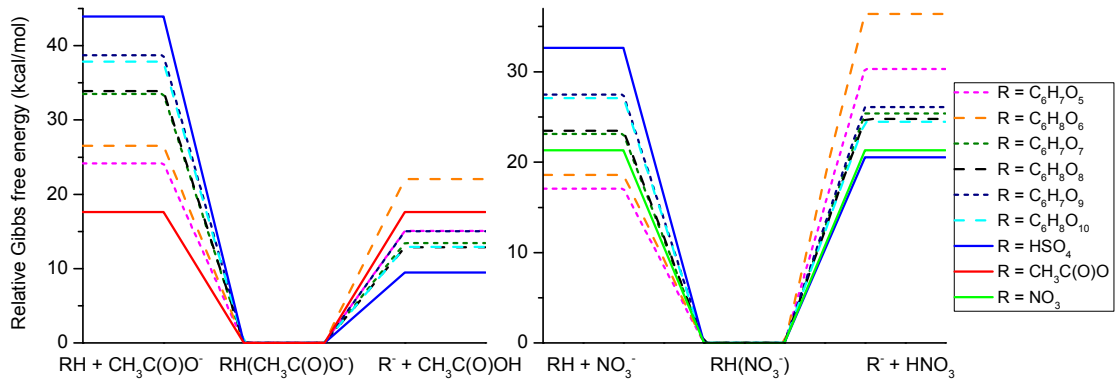

Figure 4 The free energy differences between $RH + Q^-$, $RH(Q^-)$ and $R^- + QH$ in acetate (left panel) and nitrate (right panel) chemical ionization.

DISCUSSION AND CONCLUSIONS

All of the lowest-energy conformers of the clusters of the studied autoxidation products with acetate and nitrate have either one or two intermolecular hydrogen bonds between the sample molecule and the reagent ion, even though $C_6H_8O_9$ and $C_6H_9O_{10}$ both have three hydrogen

bonding hydroperoxy groups. This indicates that these reagent ions do not form more than two hydrogen bonds that are stronger than the intramolecular hydrogen bonds of the sample molecules. The small increase in the binding energies of the molecules that have an additional hydroperoxy group (going from $C_6H_9O_8$ to $C_6H_9O_{10}$, and from $C_6H_8O_7$ to $C_6H_8O_9$) can be explained by the intramolecular hydrogen bond between the hydroperoxy group and one of the peroxy acid groups. The additional hydrogen bond between the hydroperoxy group and the peroxy acid helps polarize the acid group, thus slightly increasing its binding to the reagent ion. Increasing the number of hydroperoxy groups beyond two will thus probably not make a large difference to the binding energies of the clusters.

The calculations agree with the measurements[25] that show a high detection efficiency for also the less oxidized sample molecules using acetate chemical ionization. Using acetate, the ligand exchange reactions are favorable for all of the studied molecules. Using nitrate, the ligand exchange reactions are much less favorable (or even unfavorable for the less oxidized sample molecules, $C_6H_9O_6$ and $C_6H_8O_5$) because of the strong binding of the $HNO_3(NO_3^-)$ dimer, which explains why $C_6H_8O_5$ was not detected, and $C_6H_9O_6$ was detected with a lower detection efficiency, when using nitrate. The deprotonation of some of the sample molecules in the measurements, using acetate chemical ionization, can also be explained by the calculations, as the deprotonation of all of the sample molecules is more favorable than fragmentation into RH + Q^-. Our calculations also explain why acetate and nitrate have similar sensitivities for cyclohexene autoxidation products with elemental formulae $C_6H_9O_8$ and $C_6H_9O_{10}$. The only experimental result that we could not directly explain is the slightly lower detection efficiency of $C_6H_8O_9$ using acetate than using nitrate.[25,28] One possible reason for this might lie in the ability of acetate to deprotonate many of the highly oxidized molecules. It is possible that some of the

deprotonated molecules are lost (i.e. remain undetected) if they are able to bind strongly with other neutral molecules in the sample flow.

The energy of R^- + QH has to be lower than the energy of RH + Q^- to make deprotonation more favorable than fragmentation into RH + Q^-. Our calculations show that acetate is able to deprotonate all of the highly oxidized cyclohexene ozonolysis products. However, the energy difference between the R^- + QH and the cluster RH(Q^-) of the different molecules varies, likely making the deprotonation-to-clustering signal ratios different. Especially the intramolecular hydrogen bonds in the deprotonated molecules make the deprotonation significantly more favorable than fragmentation into RH + Q^-. The addition of hydroperoxy groups in the molecule decreases the energy needed to deprotonate the molecule, if the hydroperoxy group(s) of the deprotonated ion are able to form intramolecular hydrogen bonds with the O_2^- group.

Nitrate-based CIMS instruments are known to deprotonate H_2SO_4 despite the deprotonation reaction $H_2SO_4(NO_3^-) \rightarrow HSO_4^- + HNO_3$ requiring considerable energy (20.5 kcal/mol in terms of the standard Gibbs free energy). Based on the energetics and the vibrational modes of the $H_2SO_4 + NO_3^-$ system, our simulations indicate that the $H_2SO_4(NO_3^-)$ clusters are very likely collisionally stabilized under atmospheric conditions, as well as in the ion-molecule reaction region of the CIMS instrument. This means that the deprotonation of H_2SO_4 should not occur during the chemical ionization step itself, but rather occurs in the subsequent passage through the instrument (e.g. due to high-energy collisions in the ion optics). Determining the conditions where the sample molecules are deprotonated by the reagent ions would require a detailed modeling of the whole CIMS instrument (including inherently non-thermal high-energy conditions) and is outside the scope of this study. Assuming that deprotonation depends only on the energy differences (as observed for declustering in the case of iodide-CIMS instruments[40]),

other molecules that have deprotonation energetics similar to, or more favorable than, H_2SO_4 should thus also be susceptible to deprotonation inside CIMS instruments. This means that at least the sample molecules for which the free energy difference between R^- + QH and the cluster is less than 20.5 kcal/mol, and for which the R^- + QH energy lies below the RH + Q^- energy, should be detectable as deprotonation products, in addition to $(RH)Q^-$ clusters. Molecules with higher deprotonation energies may be bound so strongly to the reagent ions that they do not necessarily fragment inside the instrument even when R^- + QH is lower in energy than the RH + Q^-. Of the molecules and the reagent ions studied here, all except the least oxidized RO_2 radical, $C_6H_9O_6$, should be deprotonated using acetate chemical ionization, while only H_2SO_4 is likely to be deprotonated using nitrate.

ASSOCIATED CONTENT

Supporting Information. Table S1 DLPNO-CCSD(T) corrections to the ωB97xD/aug-cc-pVTZ level formation electronic energies of the closed-shell species. Table S2 Absolute ωB97xD/aug-cc-pVTZ level Gibbs free energies, enthalpies, and zero-point energies of the neutral molecules, anions and clusters. Section S1. The lowest-energy structures. This material is available free of charge via the Internet at http://pubs.acs.org.

AUTHOR INFORMATION

Corresponding Author

*E-mail: theo.kurten@helsinki.fi. Tel: +358 50 526 0123.

Author Contributions

The manuscript was written through contributions of all authors. All authors have given approval to the final version of the manuscript.

ACKNOWLEDGMENT

We thank Dr. Torsten Berndt and Ass. Prof. Mikael Ehn for helpful discussions on the experimental results related to this study. We thank the Academy of Finland for funding and CSC-IT Center for Science in Espoo, Finland, for computing time.

REFERENCES

(1) Stocker, T.F.; Qin, D.; Plattner, G.-K.; Tignor, M.; Allen, S. K.; Boschung, J.; Nauels, A.; Xia, Y.; Bex, V.; Midgley, P.M.; et al. IPCC, 2013: Summary for Policymakers. In: Climate Change 2013: The Physical Science Basis. Contribution of Working Group I to the Fifth Assessment Report of the Intergovernmental Panel on Climate Change. Cambridge University Press, Cambridge, United Kingdom and New York, NY, USA, 2013.

(2) Kanakidou, M.; Seinfeld, J. H.; Pandis, S. N.; Barnes, I.; Dentener, F. J.; Facchini, M. C.; Van Dingenen, R.; Ervens, B.; Nenes, A.; Nielsen, C. J.; et al. Organic Aerosol and Global Climate Modelling: A Review. *Atmos. Chem. Phys.* **2005,** *5*, 1053-1123.

(3) Allan, J. D.; Alfarra, M. R.; Bower, K. N.; Coe, H.; Jayne, J. T.; Worsnop, D. R.; Aalto, P. P.; Kulmala, M.; Hyötyläinen, T.; Cavalli, F.; et al. Size and Composition Measurements of Background Aerosol and New Particle Growth in a Finnish Forest During QUEST 2 Using an Aerodyne Aerosol Mass Spectrometer, *Atmos. Chem. Phys.* **2006,** *6*, 315-327.

(4) Hallquist, M.; Wenger, J. C.; Baltensperger, U.; Rudich, Y.; Simpson, D.; Claeys, M.; Dommen, J.; Donahue, N. M.; George, C.; Goldstein, A. H.; et al. The Formation, Properties and Impact of Secondary Organic Aerosol: Current and Emerging Issues. *Atmos. Chem. Phys.* **2009,** *9*, 5155-5236.

(5) Nozière, B.; Kalberer, M.; Claeys, M.; Allan, J.; D'Anna, B.; Decesari, S.; Finessi, E.; Glasius, M.; Grgić, I.; Hamilton, J. F.; et al. The Molecular Identification of Organic Compounds in the Atmosphere: State of the Art and Challenges. *Chem. Rev.* **2015,** *115*, 3913-3983.

(6) Ehn, M.; Kleist, E.; Junninen, H.; Petäjä, T.; Lönn, G.; Schobesberger, S.; Dal Maso, M.; Trimborn, A.; Kulmala, M.; Worsnop, D. R.; et al. Gas Phase Formation of Extremely Oxidized Pinene Reaction Products in Chamber and Ambient Air. *Atmos. Chem. Phys.* **2012,** *12*, 5113-5127.

(7) Zhang, X.; McVay, R. C.; Huang, D. D.; Dalleska, N. F.; Aumont, B.; Flagan, R. C.; Seinfeld, J. H. Formation and Evolution of Molecular Products in α-Pinene Secondary Organic Aerosol. *Proc. Natl. Acad. Sci. U. S. A.* **2015,** *112*, 14168-14173.

(8) Tröstl, J.; Chuang, W. K.; Gordon, H.; Heinritzi, M.; Yan, C.; Molteni, U.; Ahlm, L.; Frege, C.; Bianchi, F.; Wagner, R.; et al. The Role of Low-Volatility Organic Compounds in Initial Particle Growth in the Atmosphere. *Nature* **2016,** *533*, 527-531.

(9) Goldstein, A. H.; Galbally, I. E. Known and Unexpected Organic Constituents in the Earth's Atmosphere. *Environ. Sci. Technol.* **2007,** *41*, 1514-1521.

(10) Jokinen, T.; Sipilä, M.; Junninen, H.; Ehn, M.; Lönn, G.; Hakala, J.; Petäjä, T.; Mauldin III, R. L.; Kulmala, M.; Worsnop, D. R. Atmospheric Sulphuric Acid and Neutral Cluster Measurements Using CI-APi-TOF. *Atmos. Chem. Phys.* **2012,** *12*, 4117-4125.

(11) Ehn, M.; Thornton, J. A.; Kleist, E.; Sipilä, M.; Junninen, H.; Pullinen, I.; Springer, M.; Rubach, F.; Tillmann, R.; Lee, B.; et al. A Large Source of Low-Volatility Secondary Organic Aerosol. *Nature* **2014,** *506,* 476-479.

(12) Sarnela, N.; Jokinen, T.; Nieminen, T.; Lehtipalo, K.; Junninen, H.; Kangasluoma, J.; Hakala, J.; Taipale, R.; Schobesberger, S.; Sipilä, M.; et al. Sulphuric Acid and Aerosol Particle Production in the Vicinity of an Oil Refinery. *Atmos. Environ.* **2015,** *119*, 156-166.

(13) Yan, C.; Nie, W.; Äijälä, M.; Rissanen, M. P.; Canagaratna, M. R.; Massoli, P.; Junninen H.; Jokinen, T.; Sarnela, N.; Häme, S. A. K.; et al. Source Characterization of Highly Oxidized Multifunctional Compounds in a Boreal Forest Environment Using Positive Matrix Factorization. *Atmos. Chem. Phys.* **2016,** *16*, 12715-12731.

(14) Mutzel, A.; Poulain, L.; Berndt, T.; Iinuma, Y.; Rodigast, M.; Böge, O.; Richters, S.; Spindler, G.; Sipilä, M.; Jokinen, T.; et al. Highly Oxidized Multifunctional Organic Compounds Observed in Tropospheric Particles: A Field and Laboratory Study. *Environ. Sci. Technol.* **2015,** *49*, 7754-7761.

(15) Jokinen, T.; Kausiala, O.; Garmash, O.; Peräkylä, O.; Junninen, H.; Schobesberger, S.; Yan, C.; Sipilä, M.; Rissanen, M. P. Production of Highly Oxidized Organic Compounds from Ozonolysis of β-Caryophyllene: Laboratory and Field Measurements. *Boreal Env. Res.* **2016,** *21*, 262-273.

(16) Mentel, T. F.; Springer, M.; Ehn, M.; Kleist, E.; Pullinen, I.; Kurtén, T.; Rissanen, M.; Wahner, A.; Wildt, J. Formation of Highly Oxidized Multifunctional Compounds: Autoxidation of Peroxy Radicals Formed in the Ozonolysis of Alkenes – Deduced from Structure-Product Relationship, *Atmos. Chem. Phys.* **2015,** *15*, 6745-6765.

(17) Jokinen, T.; Sipilä, M.; Richters, S.; Kerminen, V.-M.; Paasonen, P.; Stratmann, F.; Worsnop, D.; Kulmala, M.; Ehn, M.; Herrmann, H.; et al. Rapid Autoxidation Forms Highly Oxidized RO_2 Radicals in the Atmosphere. *Angew. Chem. Int. Ed.* **2014,** *53*, 14596-14600.

(18) Rissanen, M. P.; Kurtén, T.; Sipilä, M.; Thornton, J. A.; Kangasluoma, J.; Sarnela, N.; Junninen, H.; Jørgensen, S.; Schallhart, S.; Kajos, M. K.; et al. The Formation of Highly Oxidized Multifunctional Products in the Ozonolysis of Cyclohexene. *J. Am. Chem. Soc.* **2014,** *136*, 15596-15606.

(19) Chhabra, P. S.; Lambe, A. T.; Canagaratna, M. R.; Stark, H.; Jayne, J. T.; Onasch, T. B.; Davidovits, P.; Kimmel, J. R.; Worsnop, D. R. Application of High-Resolution Time-of-Flight Chemical Ionization Mass Spectrometry Measurements to Estimate Volatility Distributions of α-Pinene and Naphthalene Oxidation Products. *Atmos. Meas. Tech.* **2015,** *8*, 1-18.

(20) Yatavelli, R. L. N.; Lopez-Hilfiker, F.; Wargo, J. D.; Kimmel, J. R.; Cubison, M. J.; Bertram, T. H.; Jimenez, J. L.; Gonin, M.; Worsnop, D. R.; Thornton, J. A. A Chemical Ionization High-Resolution Time-of-Flight Mass Spectrometer Coupled to a Micro Orifice Volatilization Impactor (MOVI-HRToF-CIMS) for Analysis of Gas and Particle-Phase Organic Species. *Aerosol Sci. Technol.* **2012,** *46*, 1313-1327.

(21) Veres, P.; Roberts, J. M.; Warneke, C.; Welsh-Bon, D.; Zahniser, M.; Herndon, S.; Fall, R.; de Gouw, J. Development of Negative-Ion Proton-Transfer Chemical-Ionization Mass Spectrometry (NI-PT-CIMS) for the Measurement of Gas-Phase Organic Acids in the Atmosphere. *Int. J. Mass Spectrom.* **2008,** *274*, 48-55.

(22) Bertram, T. H.; Kimmel, J. R.; Crisp, T. A.; Ryder, O. S.; Yatavelli, R. L. N.; Thornton, J. A.; Cubison, M. J.; Gonin, M.; Worsnop, D. R. A Field-Deployable, Chemical Ionization Time-of-Flight Mass Spectrometer. *Atmos. Meas. Tech.* **2011,** *4*, 1471-1479.

(23) Brophy, P.; Farmer, D. K. Clustering, Methodology, and Mechanistic Insights into Acetate Chemical Ionization Using High-Resolution Time-of-Flight Mass Spectrometry. *Atmos. Meas. Tech.* **2016,** *9*, 3969-3986.

(24) Hyttinen, N.; Kupiainen-Määttä, O.; Rissanen, M. P.; Muuronen, M.; Ehn, M.; Kurtén, T. Modeling the Charging of Highly Oxidized Ozonolysis Products Using Nitrate-Based Chemical Ionization. *J. Phys. Chem. A* **2015,** *119*, 6339-6345.

(25) Berndt, T.; Richters, S.; Kaethner, R.; Voigtländer, J.; Stratmann, F.; Sipilä, M.; Kulmala, M.; Herrmann, H. Gas-Phase Ozonolysis of Cycloalkenes: Formation of Highly Oxidized RO_2 Radicals and Their Reactions with NO, NO_2, SO_2, and Other RO_2 Radicals. *J. Phys. Chem. A* **2015,** *119*, 10336-10348.

(26) Berndt, T.; Richters, S.; Jokinen, T.; Hyttinen, N.; Kurtén, T.; Otkjær, R. V.; Kjaergaard, H. G.; Stratmann, F.; Herrmann, H.; Sipilä, M.; et al. Hydroxyl Radical-Induced Formation of Highly Oxidized Organic Compounds. *Nat. Commun.* **2016**, *7,* 13677.

(27) Richters, S.; Herrmann, H.; Berndt, T. Different Pathways of the Formation of Highly Oxidized Multifunctional Organic Compounds (HOMs) from the Gas-Phase Ozonolysis of β-Caryophyllene. *Atmos. Chem. Phys.* **2016,** *16*, 9831-9845.

(28) Richters, S.; Herrmann, H.; Berndt, T. Highly Oxidized RO_2 Radicals and Consecutive Products from the Ozonolysis of Three Sesquiterpenes. *Environ. Sci. Technol.* **2016,** *50*, 2354-2362.

(29) Iyer, S.; Lopez-Hilfiker, F.; Lee. B. H.; Thornton, J. A.; Kurtén, T. Modeling the Detection of Organic and Inorganic Compounds Using Iodide-Based Chemical Ionization. *J. Phys. Chem. A* **2016,** *120*, 576-587.

(30) Jørgensen, S.; Knap, H. C.; Otkjær, R. V.; Jensen, A. M.; Kjeldsen, M. L. H.; Wennberg, P. O.; Kjaergaard, H. G. Rapid Hydrogen Shift Scrambling in Hydroperoxy-Substituted Organic Peroxy Radicals. *J. Phys. Chem. A* **2016,** *120*, 266-275.

(31) *Spartan ´14*; Wavefunction, Inc.: Irvine, CA, 2014.

(32) Møller, K. H.; Otkjær, R. V.; Hyttinen, N.; Kurtén, T.; Kjaergaard, H. G. Cost-Effective Implementation of Multi-Conformer Transition Theory for Peroxy Radical Hydrogen Shift Reactions, *J. Phys. Chem. A* **2016,** *120*, 10072-10087.

(33) Frisch, M. J.; Trucks, G. W.; Schlegel, H. B.; Scuseria, G. E.; Robb, M. A.; Cheeseman, J. R.; Scalmani, G.; Barone, V.; Mennucci, B.; Petersson, G. A.; et al. *Gaussian 09,* Revision D.01; Gaussian, Inc.: Wallingford, CT, 2009.

(34) Dunning, T. H.; Peterson, K. A.; Wilson, A. K. Gaussian Basis Sets for Use in Correlated Molecular Calculations. X. The Atoms Aluminum Through Argon Revisited. *J. Chem. Phys.* **2001,** *114*, 9244-9253.

(35) Feller, D. The Role of Databases in Support of Computational Chemistry Calculations. *J. Comp. Chem.* **1996,** *17*, 1571-1586.

(36) Schuchardt, K. L.; Didier, B. T.; Elsethagen, T.; Sun, L.; Gurumoorthi, V.; Chase, J.; Li, J.; Windus, T. L. Basis Set Exchange: A Community Database for Computational Sciences. *J. Chem. Inf. Model.* **2007,** *47*, 1045-1052.

(37) Neese, F. The ORCA Program System. *Wiley Interdiscip. Rev. Comput. Mol. Sci.* **2012,** *2*, 73-78.

(38) Glowacki, D. R.; Liang, C.-H.; Morley, C.; Pilling, M. J.; Robertson, S. H. MESMER: Open-Source Master Equation Solver for Multi-Energy Well Reactions. *J. Phys. Chem. A* **2012,** *116,* 9545-9560.

(39) Hyttinen, N.; Knap, H. C.; Rissanen, M. P.; Jørgensen, S.; Kjaergaard, H. G.; Kurtén, T. Unimolecular HO_2 Loss from Peroxy Radicals Formed in Autoxidation Is Unlikely under Atmospheric Conditions. *J. Phys. Chem. A* **2016,** *120*, 3588-3595.

(40) Lopez-Hilfiker, F. D.; Iyer, S.; Mohr, C.; Lee, B. H.; D'Ambro, E. L.; Kurtén, T.; Thornton, J. A. Constraining the Sensitivity of Iodide Adduct Chemical Ionization Mass Spectrometry to Multifunctional Organic Molecules Using the Collision Limit and Thermodynamic Stability of Iodide Ion Adducts. *Atmos. Meas. Tech.* **2016**, *9*, 1*505-1512.*

TOC Graphic

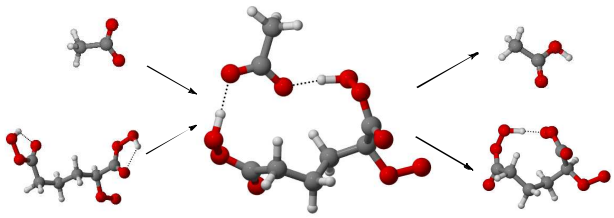

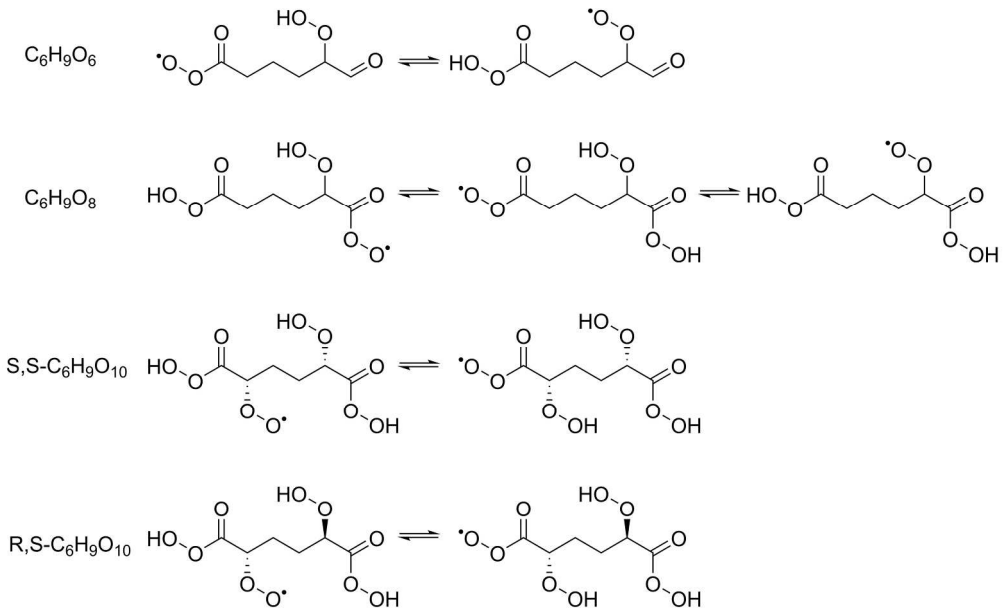

Figure 1 Cyclohexene ozonolysis derived highly oxidized RO2 radicals by Rissanen et al.18 on the left column (C6H9O6, C6H9O8, S,S-C6H9O10, and R,S-C6H9O10). On the right are the possible products of rapid H-shift scrambling reactions.

103x62mm (600 x 600 DPI)

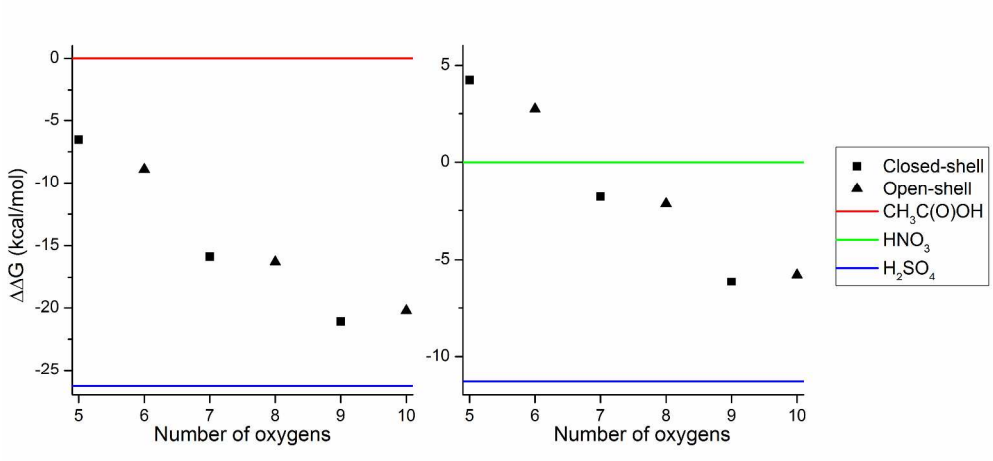

Figure 2 ωB97xD/aug-cc-pVTZ level formation free energies of the acetate (left panel) and nitrate (right panel) clusters, relative to the reagent ion dimer QH(Q-), in kcal/mol.

381x177mm (300 x 300 DPI)

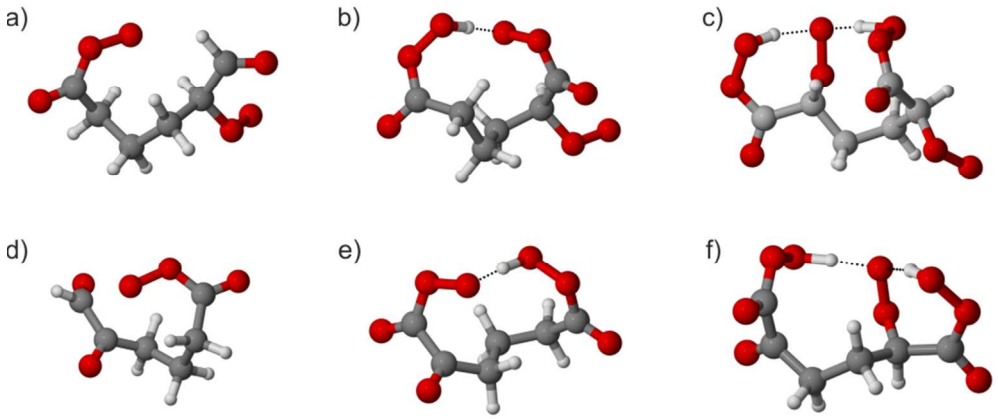

Figure 3 The lowest-energy structures of the deprotonated RO2 radicals (the peroxy radical groups are on the bottom right corners of the individual structures), a) $C_6H_8O_6^-$, b) $C_6H_8O_8^-$, c) $C_6H_8O_{10}^-$ and closed-shell species, d) $C_6H_7O_5^-$, e) $C_6H_7O_7^-$, f) $C_6H_7O_9^-$. Color coding: grey = carbon, red = oxygen, and white = hydrogen.

82x36mm (300 x 300 DPI)

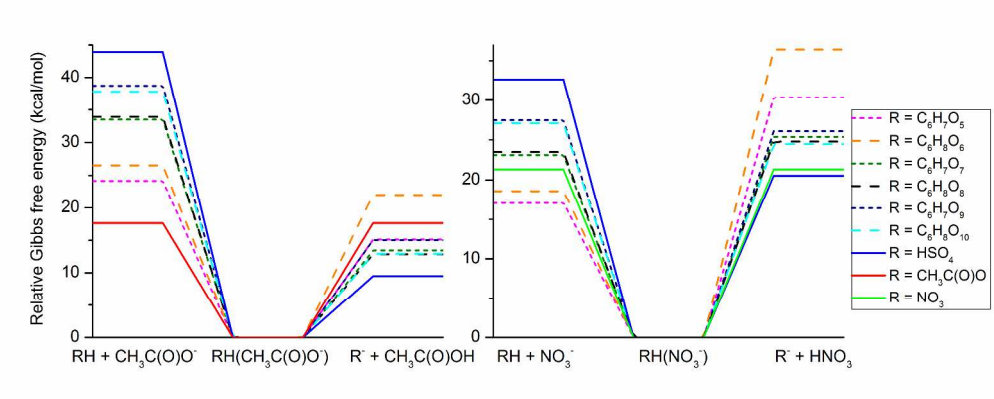

Figure 4 The free energy differences between RH + Q-, RH(Q-) and R- + QH in acetate (left panel) and nitrate (right panel) chemical ionization.

381x152mm (300 x 300 DPI)

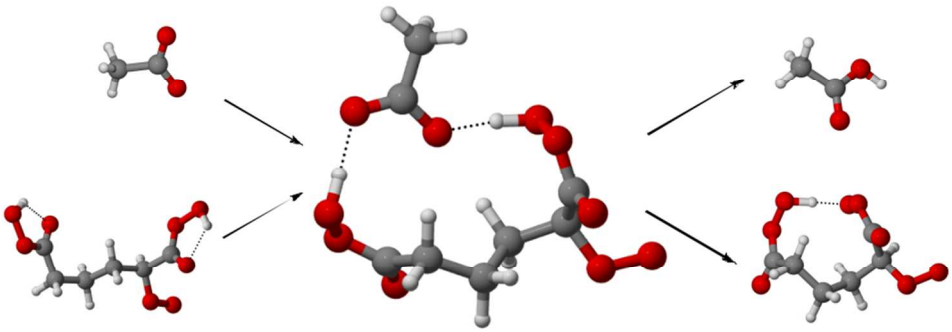

TOC image

85x31mm (300 x 300 DPI)